



UNIVERSITY OF LEEDS

This is a repository copy of *Electrochemical Insight into the Brust-Schiffrin Synthesis of Au Nanoparticles*.

White Rose Research Online URL for this paper:
<http://eprints.whiterose.ac.uk/93045/>

Version: Accepted Version

Article:

Uehara, A, Booth, SG, Chang, SY et al. (5 more authors) (2015) Electrochemical Insight into the Brust-Schiffrin Synthesis of Au Nanoparticles. *Journal of the American Chemical Society*, 137 (48). pp. 15135-15144. ISSN 0002-7863

<https://doi.org/10.1021/jacs.5b07825>

Reuse

Unless indicated otherwise, fulltext items are protected by copyright with all rights reserved. The copyright exception in section 29 of the Copyright, Designs and Patents Act 1988 allows the making of a single copy solely for the purpose of non-commercial research or private study within the limits of fair dealing. The publisher or other rights-holder may allow further reproduction and re-use of this version - refer to the White Rose Research Online record for this item. Where records identify the publisher as the copyright holder, users can verify any specific terms of use on the publisher's website.

Takedown

If you consider content in White Rose Research Online to be in breach of UK law, please notify us by emailing eprints@whiterose.ac.uk including the URL of the record and the reason for the withdrawal request.



eprints@whiterose.ac.uk
<https://eprints.whiterose.ac.uk/>

Electrochemical insight into the Brust-Schiffrin synthesis of Au nanoparticles

Akihiro Uehara,^{†,‡,*} Samuel G. Booth,[‡] Sin Yuen Chang,[§] Sven L. M. Schroeder,[⊥] Takahito Imai,[#] Teruo Hashimoto,^{||} J. Frederick W. Mosselmans,[∇] and Robert A.W. Dryfe[‡]

[†] Division of Nuclear Engineering Science, Research Reactor Institute, Kyoto University, Asashironishi, Kumatori, Osaka, 590-0494, Japan

[‡] School of Chemistry, [§] School of Chemical Engineering and Analytical Science, and ^{||} School of Materials, The University of Manchester, Oxford Road, Manchester, M13 9PL, United Kingdom

[⊥] School of Chemical and Process Engineering, Faculty of Engineering, University of Leeds, Leeds LS2 9JT, United Kingdom

[#] Department of Materials Chemistry, Faculty of Science and Technology, Ryukoku University, Otsu, Shiga 520-2194, Japan

[∇] Diamond Light Source Ltd, Didcot, Oxfordshire, OX11 0DE, United Kingdom

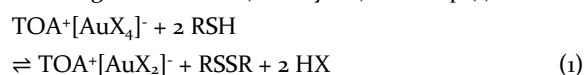
Supporting Information

ABSTRACT: The mechanism of the Brust-Schiffrin gold nanoparticle synthesis has been investigated through the use of ion transfer voltammetry at the water|1,2-dichloroethane (DCE) solution interface, combined with X-ray absorption fine structure (XAFS) of the reaction between $[\text{AuCl}_4]^-$ and thiol (RSH) in homogeneous toluene (TL) solution. Ion transfer calculations indicate the formation of $[\text{AuCl}_2]^-$ at RSH: Au ratios from 0.2 – 2 with a time-dependent variation observed over several days. At RSH: Au ratios above 2 and after time periods greater than 24 hours, the formation of Au(I)SR is also observed. The relative concentrations of reaction products observed at the liquid/liquid interface are in excellent agreement with those observed by XAFS for the corresponding reaction in a single homogeneous phase. BH_4^- ion transfer reactions between water and DCE indicate that the reduction of $[\text{AuCl}_4]^-$ and/or $[\text{AuCl}_2]^-$ to Au nanoparticles by BH_4^- proceeds in the bulk organic phase. On the other hand, BH_4^- was unable to reduce the insoluble $[\text{Au(I)SR}]_n$ species to Au nanoparticles. The number and size of the nanoparticles formed was dependent on the concentration ratio of RSH: Au, as well as the experimental duration because of the competing formation of the Au(I)SR precipitate. Higher concentrations of nanoparticles, with diameters of 1.0 – 1.5 nm, were formed at RSH: Au ratios from 1 to 2.

■ INTRODUCTION

The Brust-Schiffrin method is the earliest reported phase transfer approach to prepare thiol-stabilized metal nanoparticles¹. In this two-step approach, the gold ions from an aqueous solution are first extracted to a hydrocarbon (e.g. toluene, TL) phase using tetraoctylammonium bromide, TOA^+Br^- , as the phase transfer reagent. The phase transfer of negatively charged gold ions (e.g. tetrachloroaurate ion, $[\text{AuCl}_4]^-$) to the aqueous phase proceeds by exchange with the more hydrophilic Br^- ions in the organic phase, which are present as the counter ions of TOA^+ . Following $[\text{AuX}_4]^-$ transfer ($X = \text{halide}$) to the organic phase, the aqueous solution is discarded. Subsequent reduction reactions in the organic solution, using a second aqueous solutions of NaBH_4 in the presence of an alkanethiol added as a capping agent, yield Au nanoparticles of ~ 2.5 nm diameter. Although the Brust-Schiffrin method is extensively used and has been studied widely²⁻⁸, the synthesis process and associated mechanistic features have only recently been investigated in detail. One of the specific questions has been the identification of the precursor species pre-

sent in solution prior to reduction with NaBH_4 . In early studies of the Brust-Schiffrin process, when the precursor question was addressed, researchers generally assumed the formation of Au(I) thiolate polymers^{9,10} in both the one- and two-phase reactions, with evidence that the thiol species also functioned as reducing agents, forming Au(I) from Au(III)³. Recently, a revised view of Brust-Schiffrin nanoparticle synthesis has been pioneered by Goulet and Lennox¹¹, which indicates that the thiol (RSH) behaves solely as a reductant for $[\text{AuX}_4]^-$ before the addition of NaBH_4 , with no Au-thiol bonding observed. Au(I) reduced from Au(III) by n-dodecanethiol were shown to be precursors of one-phase reactions conducted in organic solvents (usually TL) as in Eq. (1):



The product was identified based on ¹H NMR spectroscopy and the mechanism was shown to proceed as above, with a further increase in the RSH: Au ratio above the stoichiometric ratio of equation (1) claimed to lead to the accumulation of free thiol in water-free organic solvents. A density functional theory calculation supported equation (1)¹², and a

number of experimental studies have appeared using NMR in addition to other characterization, e.g. Raman spectroscopy, and surface plasmon resonance, which have generally supported the veracity of equation (1)^{11,13-16}.

Specifically Li et al.^{13,16} have clarified that the $[\text{AuX}_2]^-$ precursor in a Brust-Schiffrin two-phase synthesis is either the $\text{TOA}^+[\text{AuX}_2]^-$ complex when $\text{RSH}:[\text{AuX}_4]^- < 2$, or a mixture of the $\text{TOA}^+[\text{AuX}_2]^-$ complex and polymeric $[\text{Au}(\text{I})\text{SR}]_n$ species when $\text{RSH}:[\text{AuX}_4]^- > 2$ in a two-phase system with water present. Saturation of the organic phase with water was claimed to lead to inverse micelles in the organic solvent, which were invoked to explain the size-specificity of the Brust-Schiffrin process¹⁶. However, the existence of inverse micelles was repudiated by Perala and co-workers¹⁷ who also developed a kinetic model based on continuous nucleation to explain the variation in particle size¹⁵. More recent NMR observations have indicated that the intermediate is reliant on the absolute concentration of the reactants as well as their ratio. Initial NMR observations agreed with those of Goulet and Lennox. However on increasing the concentrations of the reactants, soluble intermediate species, $\text{TOA}^+[\text{Au}(\text{SR})\text{X}]^-$ and $\text{TOA}^+[\text{Au}(\text{SR})_2]^-$, were also proposed¹⁸. The hypothesis being that the overall polarity of the solution and the pH is increased, reducing the suppression of halide liberation in the organic solvent. These soluble gold thiolate species were found to precipitate after a number of days. By performing the reduction with thiols of different structure it has been verified that the first two additions of thiol, required for the stoichiometric reaction, are only involved in the reduction and additional thiol may then form a bonding interaction with $\text{Au}(\text{I})$ ¹⁹. The formation of the polymeric $[\text{Au}(\text{I})\text{SR}]_n$ species depends on the reaction conditions (i.e., whether there is an aqueous layer present or not): the overall deposition process has proven to be more involved than originally believed, specifically the distribution of the reactant ions and the electron transfer between water and the organic solution will depend on the interfacial potential and electroneutrality of both phases. This means that from an electrochemical point of view, we can write the Brust-Schiffrin mechanism as summarized in Figure 1: transfer of $[\text{AuX}_4]^-$ from the aqueous phase to the organic and halide ion transfer from the organic to water (process (i)). In some studies Br^- is introduced as the counter ion to TOA^+ and there may be some substitution with the chlorine in $[\text{AuCl}_4]^-$. This may be avoided by either using TOABr and $[\text{AuBr}_4]^-$ or TOACl and $[\text{AuCl}_4]^-$ ¹¹. The reduction of $[\text{AuX}_4]^-$ either to $[\text{AuX}_2]^-$ as in Eq. (1) or polymeric $[\text{Au}(\text{I})\text{SR}]_n$ complex by addition of RSH are shown as process (ii) and (iii) respectively. The formation of polymeric $[\text{Au}(\text{I})\text{SR}]_n$ is concomitant with the distribution of H^+ and X^- from the organic to aqueous phase. Following the formation of $\text{Au}(\text{I})$, NaBH_4 is added to reduce the $\text{Au}(\text{I})$ intermediate(s) to metallic gold. This either occurs as a heterogeneous redox reaction between organic phase $[\text{AuX}_4]^-$, $[\text{AuX}_2]^-$ and/or polymeric $[\text{Au}(\text{I})\text{SR}]_n$ complexes and aqueous phase NaBH_4 or as a homogeneous redox reaction in the organic phase between those ionic gold species and BH_4^- , which has transferred from the aqueous to the organic phase (process (iv)). To maintain the electroneutrality of both phases, Cl^- formed from Au chloro-complexes should transfer from the organic to aqueous phase as a common ion. Electrochemically-controlled ion and/or electron transfer reactions have been used to probe metal deposition at the liquid-liquid interface²⁰⁻²⁸. Ion or electron transfer at the interface is observed at a potential which is dependent on the

Gibbs energy of transfer of the ions or differences of redox potential between reductant and oxidant sequestered in either phase²⁹. By measuring the redox potential of Au and appropriate reductants, as well as the Gibbs energy of ion transfer, effective metal deposition systems have been proposed^{30,31}. For the specific case of Au distribution across the liquid-liquid interface, electrochemical ion transfer of $[\text{AuCl}_4]^-$ ^{24,26,32,33} and $[\text{AuCl}_2]^-$ ³³ has been reported.

Key to a detailed understanding of the Brust-Schiffrin process is the ability to prove the oxidation state and coordination of the Au in the organic and aqueous phases. X-ray absorption fine structure (XAFS) is an ideal approach to obtain such information: numerous XAFS studies of the coordination structure of Au complexes have been carried out³⁴⁻³⁹, including the identification of valency in the reaction of Au and dodecanethiol from the X-ray absorption near-edge structure

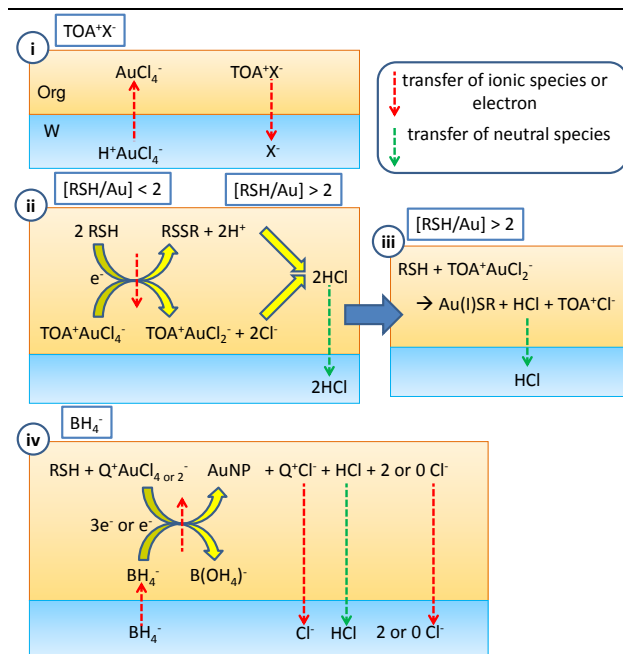


Figure 1. Brust-Schiffrin nanoparticle deposition processes. (i) ion exchange process, (ii) and (iii) reaction process between Au chloride ions with RSH, (iv) reduction of Au chloride ions by BH_4^- .

(XANES) and the characterization of Au-Cl and Au-S bonds through the analysis of the extended X-ray absorption fine-structure, EXAFS⁴⁰⁻⁴³.

In the present study, the Brust-Schiffrin nanoparticle preparation method is investigated by voltammetry for charge transfer at the interface between two immiscible electrolyte solutions (ITIES), XANES and transmission electron microscopy (TEM). As metal precursors, $[\text{AuCl}_4]^-$ and $[\text{AuCl}_2]^-$ salts were used in the presence of RSH in 1,2-dichloroethane, DCE, and toluene, TL. To avoid the formation of mixed halide gold complexes, Tetraoctylammonium chloride, TOA^+Cl^- , was used instead of TOA^+Br^- . We analyzed the processes proposed in Figure 1 by changing the holding time before the measurement and the concentration ratio of $\text{RSH}:\text{Au}$. Based on the ion transfer reaction obtained in the measurement, the effect of the holding time and the $\text{RSH}:\text{Au}$ concentration ratio on the nanoparticle formation by the reductant borohydride was also discussed and important mechanistic insights obtained.

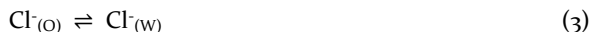
■ RESULTS AND DISCUSSION

Ion exchange reaction of $[\text{AuCl}_4]^-$ from water and the Cl^- of TOA^+Cl^- from DCE. $\text{TOA}^+[\text{AuCl}_4]^-$ in DCE has been prepared by a shake flask method using TOA^+Cl^- in DCE and $\text{H}^+[\text{AuCl}_4]^-$ in aqueous solution as in the Brust - Schiffrin method¹. In order to understand process (i) (Figure 1), we measured the ion transfer of $[\text{AuCl}_4]^-$ from water to organic DCE at the micro-interface as shown in the voltammetric response (a) of Figure 2. For the case of the anions shown here, increasing potentials of transfer indicate increasing lipophilicity. The diffusion current was proportional to the concentration of $[\text{AuCl}_4]^-$ from 0.1 to 1 mM, indicating that the current was controlled by the diffusion of $[\text{AuCl}_4]^-$ in water. The half-wave potential for the transfer as shown in Eq. (2) was calculated to be 0.115 V.



An acidified aqueous phase (10 mM HCl) was used to avoid the partial hydrolysis of $[\text{AuCl}_4]^-$ which occurs in aqueous solutions at high pH⁴⁴. The presence of $[\text{Au}(\text{OH})\text{Cl}_3]^-$ and $[\text{Au}(\text{OH})_2\text{Cl}_2]^-$ would affect the reduction by RSH and subsequent particle formation because of the different reduction potentials of the hydrolyzed complexes which are relatively more hydrophilic. The transfer of $[\text{AuCl}_4]^-$ (dissolved in DCE as $\text{TOA}^+[\text{AuCl}_4]^-$) from DCE to water was observed as a positive current as shown in curves (b) of Figure 2. The transfer potential was identical with the transfer of $[\text{AuCl}_4]^-$ (dissolved as HAuCl_4) from water to DCE. As these two species were indistinguishable all subsequent experimental work utilized $\text{TOA}^+[\text{AuCl}_4]^-$ which is soluble in the organic phase, instead of repeating the phase transfer process.

When TOA^+Cl^- (the phase transfer catalyst in the Brust-Schiffrin reaction) was dissolved in DCE, the transfer of Cl^- from DCE to water was observed at the negative end of the potential window (transfer potential of -0.32 V) as shown in curve (d) in Figure 2 (Eq. (3)):



In the preparation of $\text{TOA}^+[\text{AuCl}_4]^-$, the aforementioned ion exchange between Cl^- in organic and $[\text{AuCl}_4]^-$ in water (process (i)) proceeds spontaneously based on the Gibbs energies for the transfer of Cl^- ^{45,46} and $[\text{AuCl}_4]^-$ ³³ and their concentrations. Here, the phase boundary potential⁴⁷, which is defined by the transfer of Cl^- present in excess as TOA^+Cl^- in

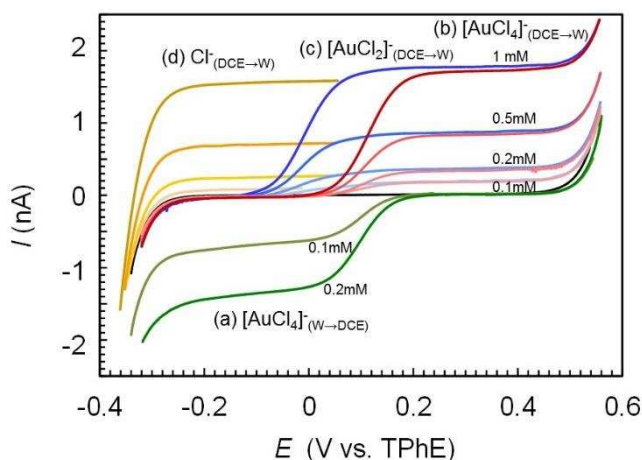


Figure 2. Voltammograms for the transfer of $[\text{AuCl}_4]^-$, $[\text{AuCl}_2]^-$, and Cl^- between water and DCE. Curves (a); 0.1, 0.2 mM $\text{H}^+[\text{AuCl}_4]^-$ in water, curves (b); 0.1, 0.2, 0.5, 1 mM $\text{TOA}^+[\text{AuCl}_4]^-$ in DCE, curves (c); 0.1, 0.2, 0.5, 1 mM $\text{TOA}^+[\text{AuCl}_2]^-$ in DCE, (d); 0.1, 0.2, 0.5, 1 mM TOA^+Cl^- in DCE. The potential scanning rate was 5 mV s^{-1} .

the organic solution and $[\text{AuCl}_4]^-$ in water before equilibrium has been reached, determines the distribution of ionic species between water and the organic phase. The phase boundary potential is shifted to a negative potential due to the presence of organic phase TOA^+ and concentration of Cl^- in the two phases at equilibrium. This phase boundary potential prevents the loss of Au-containing ionic species into the aqueous phase as it is below that required for Au ion transfer. In the case of the TOA^+Br^- , which has also been used as a catalyst to transfer gold into the organic phase in the Brust - Schiffrin method, ion exchange proceeds as in process (i) though Br^- is rather hydrophobic^{45,46}. By contrast, TOA^+ and H^+ do not transfer between water and DCE because of their respective hydrophobicity and hydrophilicity⁴⁵, although a specific interaction between TOA^+ and $[\text{AuCl}_4]^-$ has recently been proposed⁴⁸.

Chemical and electrochemical reaction between $[\text{AuCl}_4]^-$ and RSH: Time dependence. The second step in the Brust-Schiffrin synthesis - the reaction between $\text{TOA}^+[\text{AuCl}_4]^-$ and RSH in DCE before the addition of BH_4^- was studied using a macroscopic ITIES. Insoluble thiolate has been shown to form at the water-organic interface when the aqueous phase is retained during the thiol addition³. However, the extent of insoluble thiolate formation has not been quantified. Cyclic voltammograms were measured for the transfer of $[\text{AuCl}_4]^-$ between water and DCE containing 0.2 mM $\text{TOA}^+[\text{AuCl}_4]^-$ in the absence of RSH as shown in Figure 3 (A). Immediately after adding 0.1 mM RSH (20 μL of 10 mM RSH) into 2 mL DCE, the cyclic voltammogram was measured. The

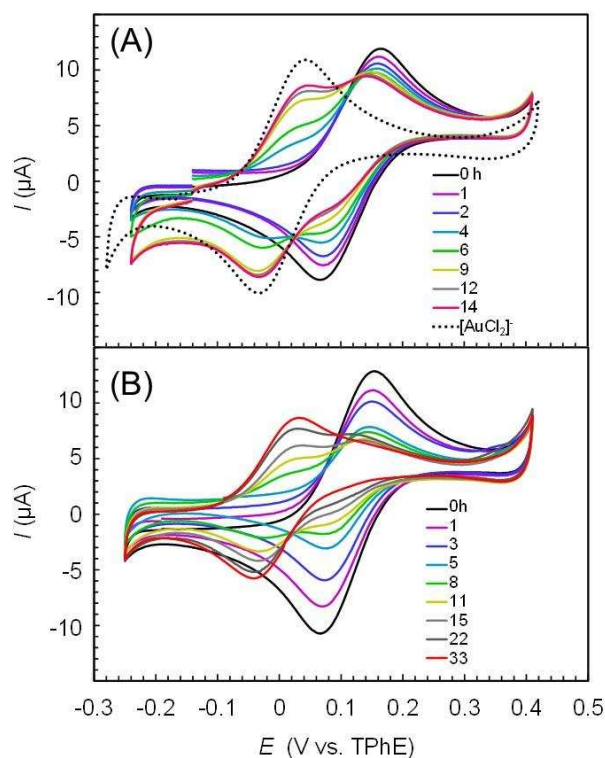
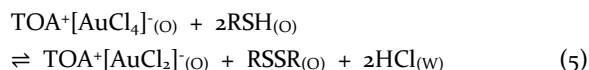


Figure 3. Time dependence on the reaction of $[\text{AuCl}_4]^-$ with RSH. Voltammogram at the macro-interface between 10 mM HCl in water and 0.2 mM $\text{TOA}^+[\text{AuCl}_4]^-$ with added (A) 0.1 mM RSH + 10 mM $\text{TOA}^+\text{TFPB}^-$ and (B) 0.4 mM RSH + 10 mM $\text{TOA}^+\text{TFPB}^-$. Dotted line in (a) shows the transfer of $[\text{AuCl}_4]^-$ in the absence of thiol as a standard. The potential scan rate was 10 mV s^{-1} .

transfer current indicative of the concentration of $[\text{AuCl}_4]^-$ began to decrease after the RSH addition. 3 hours later, a new pair of voltammetric peaks were observed at 0.002 and -0.065 V. The transfer potentials in Figure 3(A) with a new peak at -0.005 V was identified as the transfer of $[\text{AuCl}_2]^-$ ³³ as per Eq. (4). For comparison, the transfer of $[\text{AuCl}_2]^-$ in the absence of thiol is included as a dotted line in Figure 3(A).



The $[\text{AuCl}_2]^-$ peak current increased with time indicating the build-up of Au(I) until a near constant current was reached after 17 hours. The decrease of the Au(III) peak mirrors the increase in the Au(I) peak indicating that Au(III) is being directly converted into Au(I). $[\text{AuCl}_2]^-$ was formed by the oxidation of RSH to RSSR disulfide in the DCE phase, consistent with the process described in Eq.(5)¹¹ and process (ii) in Figure 1:



Here, the HCl by-product transfers from DCE to water, the dissociation constant of the acid in the organic phase can explain the lack of observed ion transfer current. We note that Duong *et al* have also studied this process using octanethiol as the reducing agent⁴⁸. They saw only a small change in the $[\text{AuCl}_4]^-$ transfer current, although the thiol was added to the aqueous phase and the time-scale of the reaction with thiol was not clear

When the concentration of RSH is higher than that of $[\text{AuCl}_4]^-$, i.e., 0.4 mM RSH and 0.2 mM $[\text{AuCl}_4]^-$, the time dependent $[\text{AuCl}_4]^-$ voltammetry evolved distinctly from the case of lower RSH concentration described above (0.1 mM RSH). Voltammograms were measured from 0 to 33 hours after RSH addition to DCE as shown in Figure 3(B). Though the transfer current of $[\text{AuCl}_4]^-$ decreased over a period from 0.5 to 6 hours, the transfer current of the $[\text{AuCl}_2]^-$ reduction product, indicated above, was not observed here. Unlike Figure 3(A) where a symmetrical voltammogram resulted from the interconversion of species, the transfer current due to $[\text{AuCl}_2]^-$ following Eq. (5) was only seen after 6 hours. These results show that about 50% of the total concentration of Au did not form $[\text{AuCl}_2]^-$, but another product resulted, which was not observed in the voltammogram at the macro-interface. The concentration dependence observed above is investigated in the next section to confirm the identity of the new species and quantify the role of RSH.

Chemical and electrochemical reaction between $[\text{AuCl}_4]^-$ and RSH: Concentration dependence of RSH. The voltammogram was recorded at the micro-interface between water, containing 10 mM HCl as supporting electrolyte, and the DCE containing various concentration ratios of Au and RSH (ratio of RSH/ $[\text{AuCl}_4]^-$: $r = 0, 0.4, 1, 2, 3, 4$, and 8). The voltammograms were measured over a period of 5 days (Figure 4 (A) - (D)). Here, the initial $[\text{AuCl}_4]^-$ concentration was 0.5 mM. The measurements were performed at different time periods: right after the preparation of the solutions, and after 1, 2, and 5 days.

As observed previously¹³, a white precipitate rapidly accumulated at the interface between W and DCE when $r \geq 2$. The presence of the precipitate blocks the interface reducing the ion transfer currents⁴⁹. To avoid this phenomenon the pelucid DCE phase of each sample was separated from the precipitate and contacted with a fresh aqueous solution for fur-

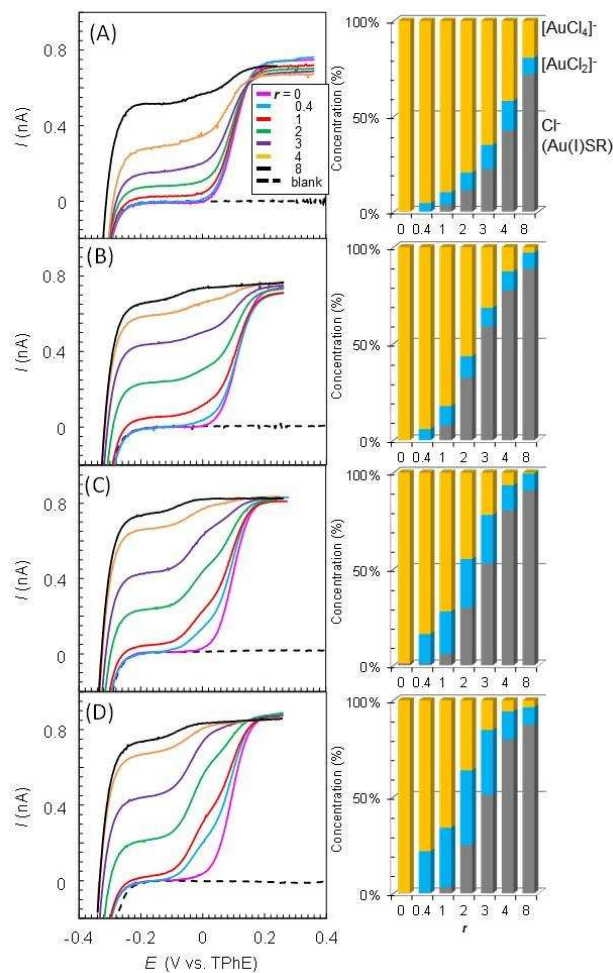
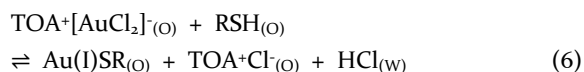
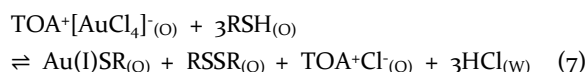


Figure 4. Effect of reaction time and RSH concentration on the reaction of $[\text{AuCl}_4]^-$ with RSH. (left) Voltammograms at the micro-interface between 10 mM HCl in water and DCE solutions containing 0.5 mM $\text{TOA}^+[\text{AuCl}_4]^-$, either 0, 0.2, 0.5, 1, 1.5, 2, or 4 mM RSH (corresponding to $r = 0, 0.4, 1, 2, 3, 4$ or 8) and 1 mM $\text{TOA}^+\text{TFPB}^-$. Voltammograms were measured directly after preparation, 1, 2, and 5 days later (A, B, C and D). The scan rate was 5 mV s^{-1} . (right) The concentrations of $[\text{AuCl}_4]^-$, $[\text{AuCl}_2]^-$, and Au(I)SR determined from the diffusion current of each species.

ther voltammetry. This is not a major concern during the duration of the experiment as the small interfacial contact area means that the system is effectively a single-phase reaction. As shown in Figure 4, three positive currents were observed; the first positive current occurs at -0.18 V, the second current at -0.01 V which is assigned to the $[\text{AuCl}_2]^-$ transfer and the third current at 0.11 V is assigned to the $[\text{AuCl}_4]^-$ transfer. The -0.18 V transfer, which was not clearly observed at the macro-interface (Figure 3), corresponds to the transfer of a more hydrophilic anion from DCE to water, or alternatively a hydrophobic cation from water to DCE. It is suggested that the current corresponds to the transfer of Cl^- dissociated from $[\text{AuCl}_2]^-$ during the formation of $[\text{Au(I)SR}]_n$ in DCE as in process (iii) in Figure 1. This is because the ion transfer potential occurs at a similar potential to those observed in curves (d) of Figure 2 which correspond to the transfer of Cl^- from TOA^+Cl^- . The proposed chemical reaction between $\text{TOA}^+[\text{AuCl}_2]^-$ and RSH is given in Eq.(6);



Here, transfer of Cl^- formed from TOA^+Cl^- in DCE was observed in the voltammogram as curve (d) in Figure 2. Whereas, in the reduction of $[\text{AuCl}_4]^-$ to $[\text{AuCl}_2]^-$ the Cl^- from $[\text{AuCl}_4]^-$ is generated in conjunction with H^+ as 2 RSH form RSSR and 2 H^+ (Equation 1) ¹¹ facilitating the formation of HCl as a hydrophilic neutral species (Figure 1 (ii)). As a result, the concentration of Cl^- transferred is identical to the concentration of Au(I)SR formed in DCE. Here, soluble Au(I)SR may form the polymeric species, $[\text{Au(I)SR}]_n$, which is visible as a white precipitate. Though it has been reported that the solubility of Au(I)SR is very low¹¹, Cl^- transfer was also observed in the absence of a visible white precipitate $[\text{Au(I)SR}]_n$. As TOA^+Cl^- remains soluble during the reaction, an accurate concentration of Au(I)SR may be measured indirectly from the Cl^- concentration after the removal of the white precipitate. The concentration ratios of $[\text{AuCl}_4]^-$, $[\text{AuCl}_2]^-$ and Cl^- calculated from the limiting currents were plotted as a function of r and time in Figure 4 (right). Here, the current corresponding to $[\text{AuCl}_2]^-$ transfer was calculated by the subtraction from the current corresponding to $[\text{AuCl}_4]^-$ as shown in Figure S1. Based on the measurements at the micro-interface it can be seen that the concentration ratio of $[\text{AuCl}_4]^-$, $[\text{AuCl}_2]^-$ and Cl^- (indirectly, Au(I)SR) were dependent on time as well as thiol to gold ratio. The concentration of $[\text{AuCl}_2]^-$ slowly increased depending on the duration of the contact time for $0.4 \leq r \leq 3$. We note that the $[\text{AuCl}_2]^-$ concentration was highest at $r = 2$, beyond this ratio the $[\text{AuCl}_2]^-$ concentration falls. The $[\text{AuCl}_2]^-$ concentration was less than 10% of the total gold immediately after the sample preparation, independent of r , whilst Cl^- transfer (related to Au(I)SR) was observed to be more than 70% at $r = 8$ (Figure 4). The concentration of Au(I)SR formed in DCE increased with the amount of thiol added. It should be noted that approximately 20% of the Au was present as Au(I)SR when $r = 2$, whereas previously it has been reported that Au(I)SR was not formed alongside $[\text{AuCl}_2]^-$ at $r = 2$, when the aqueous phase was removed¹¹. These results obtained on the time dependence of the reaction indicate that Au(I)SR could form directly from $[\text{AuCl}_4]^-$ at $r > 2$ because Au(I)SR formation was quicker than $[\text{AuCl}_2]^-$ formation as Eq.(7), as opposed to the two step-reaction in Eq. (5 and 6) and Figure 1 (i and ii).



This process was also supported by the results obtained at the macro-interface (Fig.3 (B)) where a delay is noted between the onset of $[\text{AuCl}_4]^-$ reduction and $[\text{AuCl}_2]^-$ evolution. As stated previously the Cl^- transfer indicative of Au(I)SR formation could not be detected in the macro-interfacial set up.

XAFS measurements were taken of a solution containing 5 mM $\text{TOA}^+[\text{AuCl}_4]^-$ and various equivalents of RSH in TL. At a low thiol concentration ($r = 0.5$) the solution was examined over a number of hours. It was found that there was a clear time dependence to the reaction over a timescale longer than that typically utilised in the Brust-Schiffrin synthesis, Figure 5(A). To enhance the reaction, samples were scanned with stirring at times > 10 hours after mixing. Figure 5(B) shows that the XAFS results at $r = 0.5, 1, 2$, and 5 and the linear combination fitting to pure standard spectra for $\text{TOA}^+[\text{AuCl}_4]^-$, $\text{TBA}^+[\text{AuCl}_2]^-$, $[\text{Au(I)SR}]_n$. These standards are also plotted for comparison. A solution of $\text{TOA}^+[\text{AuCl}_4]^-$ was used for Au(III), $[\text{AuCl}_2]^-$ was extracted from a solution of $\text{TBA}^+[\text{AuCl}_2]^-$ as detailed previously³⁹, and a solid spectrum of dried $[\text{Au(I)SR}]_n$ precipitate was used to examine the possible presence of gold

thiolate. Principal component analysis was performed on the data set indicating that there were three different gold species present in the system (Figure S3 and S4). The results on increasing thiol concentration clearly demonstrate an increase in the extent of reduction. As can be seen in Figure 5(C),

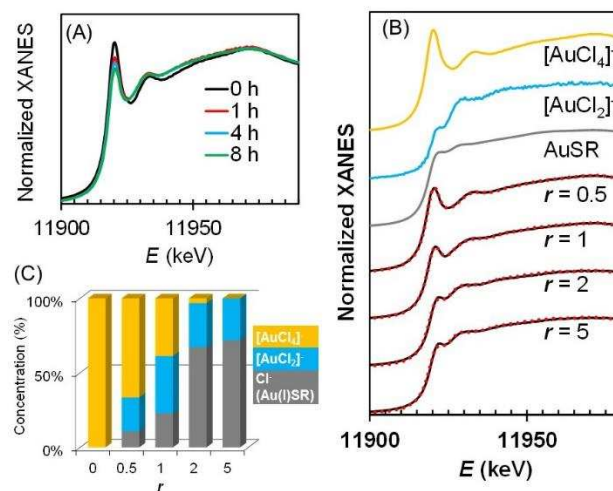


Figure 5. (A) Time dependence of the reaction at RSH: Au ratio, $r = 0.5$ showing the variation in spectra on increased reaction time. (B) Linear combination fitting (LCF) of the XANES data collected for the addition of thiol to AuCl_4^- in toluene. Solid line (experimental data), dotted line (fitting data). Normalised data sets and LCF fit for $r = 0.5, 1, 2$ and 5. The standard spectrum used for the fitting were $\text{TOA}^+[\text{AuCl}_4]^-$, $\text{TBA}^+[\text{AuCl}_2]^-$ and $[\text{Au(I)SR}]_n$. (C) Concentrations of $[\text{AuCl}_4]^-$, $[\text{AuCl}_2]^-$, and Au(I)SR were derived from the LCF.

$[\text{Au(I)SR}]_n$ is present as a component of the best fit at all thiol concentrations suggesting its formation as a minor component even below the stoichiometric ratio required for complete reduction. The initial increase in $[\text{AuCl}_2]^-$ content which then decreases suggests that the thiol may replace Cl^- as a ligand for Au(I). Figure 5(C) shows a similar ratio of products to those determined electrochemically in Figure 4(D), the samples measured at the micro-interface after 5 days.

Chemical reaction between $[\text{AuCl}_2]^-$ and RSH. The behavior of $[\text{AuCl}_2]^-$ and RSH was also studied to see if any further reactions occur following the formation of $[\text{AuCl}_2]^-$ by

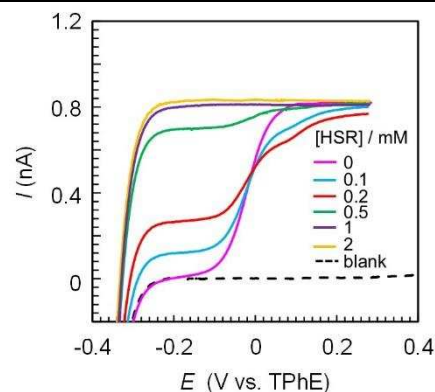


Figure 6. RSH concentration dependence on the reaction of $[\text{AuCl}_2]^-$ with RSH. Voltammograms at the micro-interface between 10 mM HCl in water and 0.5 mM $\text{TOA}^+[\text{AuCl}_2]^-$ + 0, 0.1, 0.2, 0.5, 1, and 2 mM RSH + 1 mM $\text{TOA}^+\text{TFFPB}^-$. Voltammograms were measured 1 day later. The scan rate was 5 mV s^{-1} .

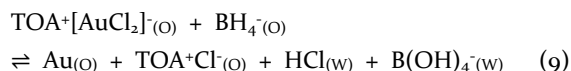
RSH. The same experimental procedure as the previous section of $[\text{AuCl}_4]^-$ experiments was used however this time $\text{TOA}^+[\text{AuCl}_2]^-$ was used instead of $\text{TOA}^+[\text{AuCl}_4]^-$ as a source of Au(I). An initial concentration of 0.5 mM $\text{TOA}^+[\text{AuCl}_2]^-$ was dissolved in DCE alongside dodecanethiol where $r = 0, 0.2, 0.4, 1, 2, \text{ and } 4$. The voltammograms obtained are shown in Figure 6. The $[\text{AuCl}_2]^-$ transfer current decreased with increasing RSH concentration. Also, the transfer of Cl^- corresponding to the formation of Au(I)SR was observed. At RSH = 1 mM, it was found that about 90% of the $[\text{AuCl}_2]^-$ species had reacted to form Au(I)SR indicating that $[\text{AuCl}_2]^-$ reacted stoichiometrically with RSH to form Au(I)SR verifying the reaction given in Equation (6). On the other hand, when the $[\text{AuCl}_2]^-$ concentration was higher than RSH i.e., $[\text{RSH}] = 0.1 \text{ and } 0.2 \text{ mM}$, $[\text{AuCl}_4]^-$ was formed as 10% of the total Au concentration through the disproportionation of Au^+ which was an intermediate species between $[\text{AuCl}_2]^-$ and Au(I)SR, and very unstable.

Deposition mechanism on the reduction of Au chloride ions by BH_4^- . The mechanism for the formation of gold nanoparticles in the presence of BH_4^- was investigated to examine the reaction process as shown in Figure 1(iv). The reaction (iv) involves reduction within the DCE bulk phase following BH_4^- transfer from water to DCE. However, alternative processes involving heterogeneous redox reactions are possible whereby $[\text{AuCl}_4]^-$, $[\text{AuCl}_2]^-$ or Au(I)SR present in the organic phase are reduced at the interface by aqueous phase BH_4^- . In order to distinguish between ion and electron transfer reactions as well as to avoid ion transfers that are not involved in the redox reaction between Au ions and BH_4^- , voltammetric measurements were performed in a bipolar cell. In this cell the aqueous and organic phases were not in direct contact but were connected by a solid electrode⁵⁰. Therefore electron transfer may be examined in the absence of any ion transfer reactions. Here, glassy carbon and platinum wire electrodes were used in water and DCE, respectively, to connect the two phases. However, no current corresponding to the electron transfer between water and DCE was observed. We therefore suggest that the ion transfer of BH_4^- from water to DCE must occur prior to undergoing homogeneous reduction of Au chloride ions within the DCE phase, Figure 1 (iv). Voltammograms were also recorded directly at the interface between water containing BH_4^- and DCE in the absence of Au chloride ions and RSH. An ion transfer current was observed at -0.3 V, the current was seen to increase with the concentration of BH_4^- as shown in Figure 7 as described in Eq. (8):



The half wave potential for the transfer of BH_4^- was calculated to be -0.36 V. Here, 1 mM LiOH was employed as a supporting electrolyte in order to avoid the decomposition of BH_4^- . This result suggests that the BH_4^- reaction with Au ions is not an interfacial one but occurs in the organic phase after the transfer from water to the organic phase (process (iv)). Although the BH_4^- ion transfers occurs at quite a negative potential because of its hydrophilicity, in the standard chemical Brust-Schiffrin process, the phase transfer may also be driven by Cl^- transfer from TOA^+Cl^- which is added in a large excess to enable the initial transfer of $[\text{AuCl}_4]^-$ from the aqueous phase to the organic⁵⁵. The transfer of BH_4^- from water to DCE overlaps with that of Cl^- (dotted line in Figure 7) resulting in the phase transfer reaction of BH_4^- and Cl^- . The phase boundary potential is negative of the Au ion transfer potential as defined by the presence of very hydrophilic ions (Cl^-) preventing the transfer of Au-containing ionic species into the aqueous

phase. Therefore, the Au ion reduction occurs in the organic phase following BH_4^- transfer from water as Eq. (9):



$[\text{AuCl}_4]^-$ may also be reduced by BH_4^- without the initial reduction by RSH¹⁶. The decomposition products of BH_4^- , e.g. to $\text{B}(\text{OH})_4^-$, has not been confirmed, therefore we have not conserved the electroneutrality of Eq. (9).

Effect of time and concentration ratio on NP formation. In order to confirm the reactivity of $[\text{AuCl}_4]^-$, $[\text{AuCl}_2]^-$ and Au(I)SR with NaBH_4 , 1 mM NaBH_4 was added to gold thiol mixtures, at a number of RSH: Au ratios, either right after sample preparation (series (A)) or 5 days after mixing (series (B)). Following the immediate addition (A), when RSH was absent, metallic gold was formed immediately in both the water and DCE phase. At 0.2 mM RSH ($r = 0.4$) the solution turned a pink color whereas a brown solution developed when 0.5 to 4 mM RSH ($r = 1 - 8$) was added to the sample which relates to the size of the particles formed. A clear absorption peak was not always observed in UV-Vis absorption spectroscopy (Figure S2(A)) TEM measurements were also performed to determine the dependence of particle size on reaction conditions as shown in the series (A) and (B) of Figure 8. The average particle diameter was 1.8 nm at $r = 0.4$, and the size slightly decreased from 1.5 to 1.0 nm for $r \geq 1$, which agrees with the variation seen in the literature in toluene systems as compiled by Perala and Kumar⁵⁵. The concentration of nanoparticles formed from solutions which were allowed to stand for 5 days was higher than those reduced initially at $r = 1 - 3$ based on the change in absorbance of the UV-Vis spectra (Figure S2(A) and (B)), although the spectroscopic data indicated that particle sizes were larger than those obtained from the fresh samples, the electron microscopy suggested the size distributions of the two sets of particles were similar. On the other hand, at a higher thiol concentration ($r = 4$ and 8) the number of particles fell progressively in the aged sample (Figure S2(B)), in marked contrast to the fresh samples at $r = 4$ and 8. On aging the reaction mixture an increase in particle size was seen from 1.8 to 2.5 nm at $r = 0.4$. This is because RSH was consumed for the reduction of $[\text{AuCl}_4]^-$ as Eq. (5). The RSH concentration at $r = 0.4$ in 5 days was calculated to be negligible small ($< 0.05 \text{ mM}$) based on the $[\text{AuCl}_2]^-$ concentration in Figure 4 (D). Particle size was critically depended on

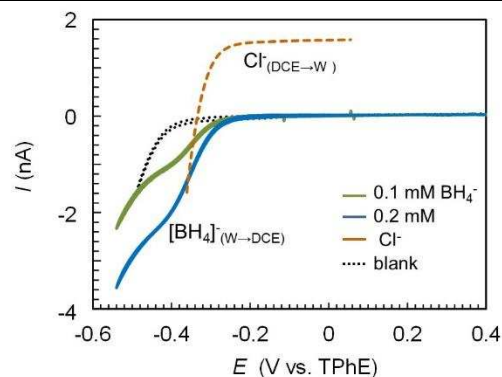


Figure 7. Voltammograms for the transfer of BH_4^- between water and DCE. Solid lines were 0, 0.1, 0.2, 0.4, 0.6 mM NaBH_4 + 1 mM LiOH in water. The dotted line shows the voltammogram for the transfer of Cl^- (1 mM TOA^+Cl^- in DCE, curve (c) in Figure 2). The potential scan rate was 5 mV s^{-1} .

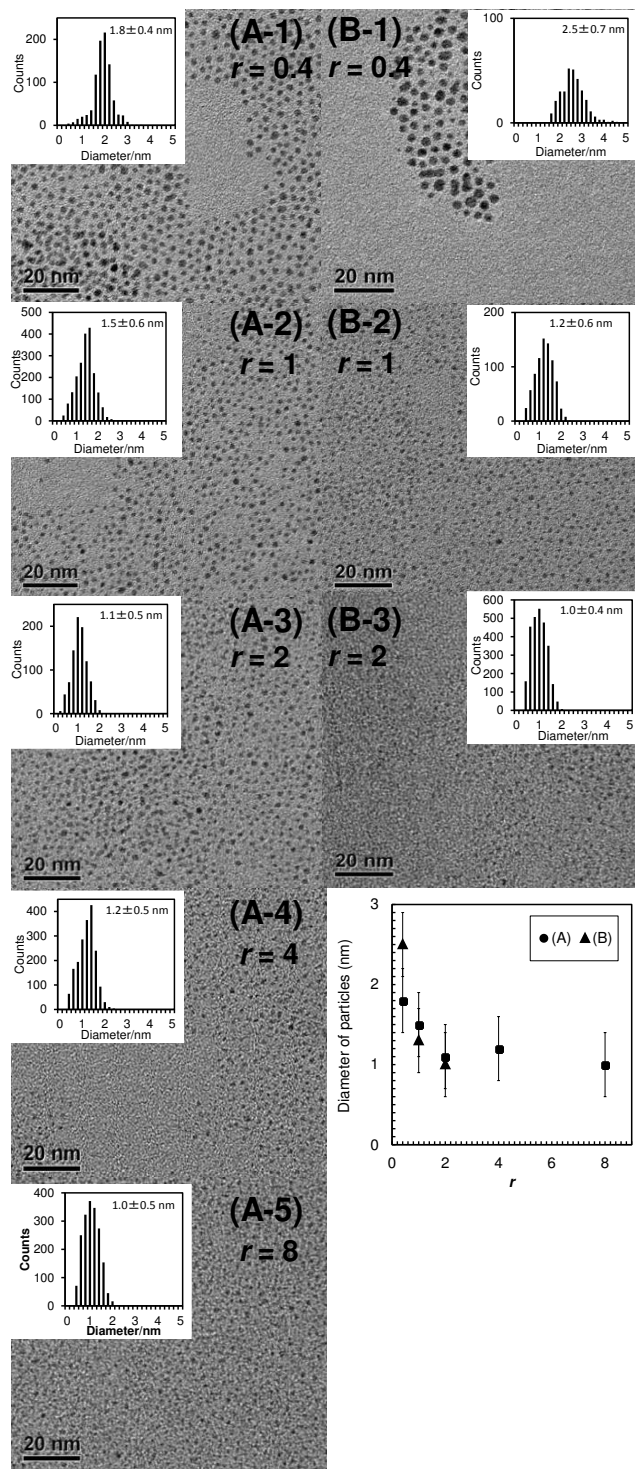


Figure 8. TEM images and size distribution after the reduction by BH_4^- . Series (A) are samples prepared by BH_4^- addition right after mixing of $[\text{AuCl}_4]^-$ and RSH ($r = 0.4 - 8$). Series (B) are samples prepared by BH_4^- addition 5 days after mixing of $[\text{AuCl}_4]^-$ and RSH ($r = 0.4 - 2$). Particle size distributions are included next to each image. The bottom right figure shows the relationship between average particle diameter and concentration ratio of RSH/Au concentration ratio.

the RSH concentration at $r = 0.4$. There was less variation in particle size from 1.0 to 1.5 nm at $r = 1$ or $r = 2$. Whereas formation of $[\text{AuCl}_2]^-$ by RSH seems to produce a higher nanoparticle concentration, a strong dependence of particle size on the relative concentrations of $[\text{AuCl}_4]^-$ and $[\text{AuCl}_2]^-$ was not observed in this study. Here, the RSH concentration remained

in 5 days were calculated to be 0.2 and 0.3 mM at $r = 1$ and $r = 2$ respectively, based on the concentrations of $[\text{AuCl}_2]^-$ and Au(I)SR. As a result, particle size from 1.0 to 1.5 nm was obtained without time depending on sample preparation. Above $r = 2$ there is little nanoparticle formation in the aged sample, suggesting that the insoluble, polymeric $[\text{Au(I)SR}]_n$ species is not readily reduced by sodium borohydride⁸. Time dependent size evolution has previously been observed following NaBH_4 addition⁹ but this is the first demonstration that the product size depends on the $[\text{AuCl}_4]^-$ and RSH mixing time.

CONCLUSIONS

The mechanistic details of the Brust-Schiffrin nanoparticle synthesis were investigated by voltammetry, XAFS, and TEM. Ion transfers related to the formation mechanism such as $[\text{AuCl}_4]^-$, $[\text{AuCl}_2]^-$, Cl^- (Au(I)SR), and BH_4^- were measured at a water | DCE interface. $\text{TOA}^+[\text{AuCl}_4]^-$ was prepared by ion exchange reaction between $[\text{AuCl}_4]^-$ in water and Cl^- in DCE (Figure 1 (i)). $[\text{AuCl}_2]^-$ was formed from the reduction of $[\text{AuCl}_4]^-$ by RSH (Figure 1 (ii)). When thiol concentration exceeded that required for the stoichiometric reaction, TOA^+Cl^- , HCl, and a white precipitate were also formed (Figure 1 (iii)). It was found that $[\text{AuCl}_2]^-$ was formed under the concentration ratio of RSH/Au $0.2 \leq r \leq 2$ and the increase in concentration was time-dependent over a period of 5 days. On the other hand, $[\text{AuCl}_2]^-$ concentration decreased at $r > 2$ after 24 hrs because of Au(I)SR formation. The concentration ratios of $[\text{AuCl}_4]^-$, $[\text{AuCl}_2]^-$ and Au(I)SR based on ion transfer currents at the ITIES were consistent with those based on XANES analysis of the corresponding homogeneous reaction. In the presence of the borohydride ion, BH_4^- , in water, the redox reaction between $[\text{AuCl}_4]^-$ and/or $[\text{AuCl}_2]^-$ and BH_4^- proceeds in DCE, following BH_4^- transfer from the aqueous phase. Cl^- , formed by the dissociation of $[\text{AuCl}_2]^-$, transferred from DCE to water to maintain electroneutrality between the two phases (Figure 1 (iv)). The insoluble form of the $[\text{Au(I)SR}]_n$ species was not reduced by BH_4^- to form nanoparticles. As can be seen from the electrochemical observations, despite the use of a liquid/liquid system in the Brust-Schiffrin synthesis all of the reduction reactions occur within the organic phase with the aqueous phase only acting as a source for $[\text{AuCl}_4]^-$ and BH_4^- . The volume and size of nanoparticles formed depended on the thiol to gold ratio as well as the mixing duration because of the $[\text{Au(I)SR}]_n$ formation. Higher concentrations of nanoparticles of 1.0 - 1.5 nm were formed for $1 \leq r \leq 2$.

EXPERIMENTAL SECTION

Chemicals. Hydrogen tetrachloroaurate, $\text{HAuCl}_4 \cdot 3\text{H}_2\text{O}$ (Alfa, $\geq 99.999\%$) was used as the source of Au(III), tetrabutylammonium dichloroaurate, $\text{TBA}^+[\text{AuCl}_2]^-$ (Tokyo Kasei, $\geq 99.99\%$) was used as the Au(I) source. HCl was used as a supporting electrolyte (WAKO Co. Ltd.) to avoid the hydrolysis of Au-chloro complex⁴⁴. 1,2-dichloroethane, DCE ($\geq 99\%$, Aldrich) and toluene, TL ($\geq 99.8\%$, Aldrich) were used as the organic solvents: these were shaken twice with deionized water because it has been reported that large quantities of water could accelerate the formation of white precipitate which was believed to be the oligomeric Au(I) thiolate species¹¹. However, the organic solutions used for electrochemistry were saturated by water as gold nanoparticles have previously been prepared using two phases in the Brust-Schiffrin method³ and the stirring required would lead to the saturation of the organic phase by water. Dodecanethiol (RSH, $\geq 98\%$, Sigma Aldrich) was used as the initial reductant. Tetroctylammonium

chloride, TOA⁺Cl⁻ (97% Sigma Aldrich) was used to generate gold salts which are stable in the organic phase. The TOA⁺ salt of [AuCl₄]⁻ was obtained as a precipitate through mixing of methanol solutions of TOA⁺Cl⁻ and HAuCl₄ and was purified by recrystallization in ethanol¹¹. The TOA⁺ salt of [AuCl₂]⁻ in DCE was prepared by shaking pure water with equimolar amounts of TBA⁺[AuCl₂]⁻ and TOA⁺Cl⁻ in DCE. The supporting electrolyte in DCE for potential sweep experiments was TOA⁺TFPB⁻ or BTPPA⁺TFPB⁻, where BTPPA⁺ and TFPB⁻ denote bis(triphenylphosphoranylidene) ammonium cation and tetrakis[3,5-bis(trifluoromethyl)phenyl] borate anion, respectively. BTPPA⁺TFPB⁻ was obtained by metathesis of BTPPA⁺Cl⁻ and Na⁺TFPB⁻⁵². Equimolar quantities of the two reactants were dissolved separately in methanol and then mixed and stirred for ~ 1 minute. The mixture was allowed to stand for 30 minutes before filtering under atmospheric conditions. The dried product was then recrystallized in ethanol.

Measurement of the voltammogram for charge transfer at the macro and micro water|DCE interfaces. Two electrochemical cells were employed; a macro-interface cell and a micro-interface cell. Cyclic voltammetry experiments were performed using a four electrode configuration with an IVIUM potentiostat (“Compactstat” model, IVIUM Technologies, the Netherlands). No iR compensation was applied for the electrochemical measurements. In the (conventional) macro-interface cell, homemade Ag/AgCl and platinum gauze were used as reference (RE) and counter (CE) electrodes respectively. The organic CE was insulated from the aqueous phase by coating its contact in a glass sheath. The cell used for the electrochemical measurements at the water|DCE interface had a cross-sectional area of about 0.64 cm² and a volume of 3 cm³. Further details are described elsewhere²⁶. The micro-interface cell uses a 16 μm thick polyester film with a micro hole of 30 μm in diameter to separate the water and DCE phases^{33–35}. The potential difference at the water|DCE interface, *E*, was measured as a function of the potential of a Ag/AgCl electrode in water. For the RE in DCE, the potential is referred to that of a BTPPA⁺ ion selective electrode, inserted in DCE. The generic cell composition is:

Ag | AgCl | 10 mM LiCl (W) | W₁ (W) || DCE₁ (DCE) | 10 mM BTPPA⁺TFPB⁻ (DCE) | 1 mM BTPPA⁺Cl⁻ + 10 mM LiCl (W) | AgCl | Ag

E is related to the Galvani potential difference, $\Delta_{DCE}^W\phi$, as shown in Eq. 10.

$$E = \Delta_{DCE}^W\phi + E_{ref} \quad (10)$$

where *E*_{ref} is the potential of the reference electrodes employed. In the calculation of $\Delta_{DCE}^WG^\circ (= -zF\Delta_{DCE}^W\phi^\circ)$, the measured *E* was converted using the extrathermodynamic assumption of Parker³⁶.

XANES measurements and analyses. XAFS spectra were acquired at the spectroscopy beamline I18 of Diamond Light Source (Harwell Science and Innovation Campus, UK). Data were acquired in fluorescence-yield mode unless otherwise stand. Intensity of the Au L₃-fluorescence emission was monitored using an Ortec multi-element solid state Ge detector³⁷. Dodecanethiol was added at RSH: Au ratios of (*r* = 0.5, 1, 2 and 5) to solutions of TOA⁺[AuCl₄]⁻ (5 mM) in TL. The solutions were mixed and allowed to stand for >10 hours before transferring to 2 mL Eppendorf tubes for XAFS measurements. TOA⁺[AuCl₄]⁻ was prepared as a standard for Au(III), the [AuCl₂]⁻ standard spectrum was generated from a species of TBA⁺[AuCl₂]⁻ spectra as discussed previously³⁹. The

[Au(I)SR]_{*n*} standard spectrum was collected at beamline B18 at the Diamond Light Source in transmission mode⁵⁸. To produce the “white precipitate” TOA⁺[AuCl₄]⁻ (4.38 mM) was mixed in a 1:5 ratio with RSH (21.9 mM) in TL. The sample was mixed thoroughly and allowed to stand for 2 hours. A 10 fold excess of methanol was then added causing a white precipitate to crash out of solution. After standing for 1 hour the mixture was centrifuged and the powder collected. The powder was washed with toluene and methanol and centrifuged a second time before drying. To collect the spectrum, 10 mg of the white precipitate was mixed with methyl cellulose and compressed into an 8 mm pellet. Elemental analysis confirmed that there was no halide content in the white precipitate formed. The XAFS spectra were analyzed by using the Athena package⁵⁹. Samples were calibrated to gold foil samples collected at the beamtime and normalized to an edge height of 1. The normalized and calibrated spectra were then used to perform linear combination fitting in Athena. The strong XANES resonance visible in the spectra at the 11,918 eV region reflects an intra-atomic electronic transition of Au 2p core electrons to unoccupied valence states with d-characters. This produced a high intensity “white line” for Au(III) due to the high 6s and 5d orbital vacancies and the lower number of vacancies in Au(I) species results in a much lower peak at the absorption edge³⁹. The high sensitivity to unoccupied valence d-states of Au allows the identification of Au oxidation state and ligands.

Nanoparticle preparation and TEM measurement. In order to examine the time dependence on the synthesized nanoparticles, TEM images of the fresh and aged sample solutions were taken. Nanoparticles were prepared by mixing TOA⁺[AuCl₄]⁻ and RSH in DCE, then either immediately or after leaving to stand for 5 days the DCE solutions were shaken with water containing NaBH₄ and 1 mM NaOH, to stabilize the borohydride solution. The DCE was then separated from the water phase and stored in a glass vial. Immediately prior to transmission electron microscopy, TEM (JEM-2100, JEOL), the nanoparticle solution was dropped on to the TEM grid (Holey carbon films on 300 mesh copper grids, Agar Scientific) to isolate the deposit. Particle diameters were calculated using the Image J software⁶⁰.

■ ASSOCIATED CONTENT

Supporting Information

Cyclic voltammogram analyses, UV-Vis absorption spectra and principal component analysis on XANES spectra. This material is available free of charge via the internet at <http://pubs.org>.

■ AUTHOR INFORMATION

Corresponding Author

auehara@rri.kyoto-u.ac.jp

Notes

The authors declare no competing financial interests.

■ ACKNOWLEDGMENTS

This research was partly supported by The Kyoto University Foundation, Japan and by Grants-in-Aid for Scientific Research (No. 25420905) from the Ministry of Education, Culture, Sports, Science and Technology, Japan. We thank Diamond Light Source Ltd for the provision of synchrotron beam-

time (award SP-8861 and SP-11293). RAWD and SLMS gratefully acknowledge financial support from the EPSRC through an EPSRC-NSF "Materials World Network" grant (EP/H047786/1). SYC gratefully acknowledges the award of a President PhD Scholarship by the University of Manchester.

■ REFERENCES

- (1) Brust, M.; Walker, M.; Bethell, D.; Schiffrin, D. J.; Whyman, R. *Journal of the Chemical Society, Chem. Commun.* **1994**, 801.
- (2) Leff, D. V.; Ohara, P. C.; Heath, J. R.; Gelbart, W. M. *J. Phys. Chem.* **1995**, *99*, 7036.
- (3) Hostetler, M. J.; Wingate, J. E.; Zhong, C. J.; Harris, J. E.; Vachet, R. W.; Clark, M. R.; Londono, J. D.; Green, S. J.; Stokes, J. J.; Wignall, et al. *Langmuir* **1998**, *14*, 17.
- (4) Shon, Y. S.; Mazzitelli, C.; Murray, R. W. *Langmuir* **2001**, *17*, 7735.
- (5) Liu, X.; Worden, J. G.; Huo, Q.; Brennan, J. R. *J. Nanosci. Nanotechnol.* **2006**, *6*, 1054.
- (6) Shimmin, R. G.; Schoch, A. B.; Braun, P. V. *Langmuir* **2004**, *20*, 5613.
- (7) Chen, S. W.; Templeton, A. C.; Murray, R. W. *Langmuir* **2000**, *16*, 3543.
- (8) Corbierre, M. K.; Lennox, R. B. *Chem. Mater.* **2005**, *17*, 5691.
- (9) Schaaff, T. G.; Shafiqullin, M. N.; Khoury, J. T.; Vezmar, I.; Whetten, R. L.; Cullen, W. G.; First, P. N.; GutierrezWing, C.; Ascensio, J.; JoseYacamán, M. J. *J. Phys. Chem. B* **1997**, *101*, 7885.
- (10) Alvarez, M. M.; Khoury, J. T.; Schaaff, T. G.; Shafiqullin, M.; Vezmar, I.; Whetten, R. L. *Chem. Phys. Lett.* **1997**, *266*, 91.
- (11) Goulet, P. J. G.; Lennox, R. B. *J. Am. Chem. Soc.* **2010**, *132*, 9582.
- (12) Barngrover, B. M.; Aikens, C. M. *J. Am. Chem. Soc.* **2012**, *134*, 12590.
- (13) Li, Y.; Zaluzhna, O.; Tong, Y. Y. *J. Langmuir* **2011**, *27*, 7366.
- (14) Li, Y.; Zaluzhna, O.; Tong, Y. Y. *J. Chem. Commun.* **2011**, *47*, 6033.
- (15) Perala, S. R. K.; Kumar, S. *Langmuir* **2013**, *29*, 9863.
- (16) Li, Y.; Zaluzhna, O.; Xu, B. L.; Gao, Y. A.; Modest, J. M.; Tong, Y. *J. Am. Chem. Soc.* **2011**, *133*, 2092.
- (17) Perala, S. R. K.; Kumar, S. *Langmuir* **2013**, *29*, 14756.
- (18) Zhu, L. L.; Zhang, C.; Guo, C. C.; Wang, X. L.; Sun, P. C.; Zhou, D. S.; Chen, W.; Xue, G. J. *Phys. Chem. C* **2013**, *117*, 11399.
- (19) Yu, C. H.; Zhu, L. L.; Zhang, R. C.; Wang, X. L.; Guo, C. C.; Sun, P. C.; Xue, G. J. *Phys. Chem. C* **2014**, *118*, 10434.
- (20) Johans, C.; Lahtinen, R.; Kontturi, K.; Schiffrin, D. J. *J. Electroanal. Chem.* **2000**, *488*, 99.
- (21) Johans, C.; Clohessy, J.; Fantini, S.; Kontturi, K.; Cunnane, V. J. *Electrochem. Commun.* **2002**, *4*, 227.
- (22) Guo, J. *Electrochem. Commun.* **2003**, *5*, 1005.
- (23) Trojaneck, A.; Langmaier, J.; Samec, Z. *J. Electroanal. Chem.* **2007**, *599*, 160.
- (24) Lepkova, K.; Clohessy, J.; Cunnane, V. J. *Electrochim. Acta* **2008**, *53*, 6273.
- (25) Li, Q.; Xie, S. B.; Liang, Z. W.; Meng, X.; Liu, S. J.; Girault, H. H.; Shao, Y. H. *Angew. Chem. Int. Edit.* **2009**, *48*, 8010.
- (26) Gründer, Y.; Ho, H. L. T.; Mosselmanns, J. F. W.; Schroeder, S. L. M.; Dryfe, R. A. W. *Phys. Chem. Chem. Phys.* **2011**, *13*, 15681.
- (27) Nieminen, J. J.; Hatay, I.; Ge, P. Y.; Mendez, M. A.; Murtomaki, L.; Girault, H. H. *Chem. Commun.* **2011**, *47*, 5548.
- (28) Booth, S. G.; Uehara, A.; Chang, S. Y.; Mosselmanns, J. F. W.; Schroeder, S. L. M.; Dryfe, R. A. W. *J. Phys. Chem. C* **2015**, *119*, 16785.
- (29) Samec, Z. *Electrochim. Acta* **2012**, *84*, 21.
- (30) Dryfe, R. A. W.; Uehara, A.; Booth, S. G. *Chem. Rec.* **2014**, *14*, 1013.
- (31) Rodgers, A. N. J.; Booth, S. G.; Dryfe, R. A. W. *Electrochem. Commun.* **2014**, *47*, 17.
- (32) Cheng, Y.; Schiffrin, D. J. *J. Chem. Soc. Faraday Trans.* **1996**, *92*, 3865.
- (33) Uehara, A.; Hashimoto, T.; Dryfe, R. A. W. *Electrochim. Acta* **2014**, *118*, 26.
- (34) Farges, F.; Sharps, J. A.; Brown, G. E. *Geochim. Cosmochim. Acta* **1993**, *57*, 1243.
- (35) Chen, X.; Chu, W. S.; Chen, D. L.; Wu, Z. H.; Marcelli, A.; Wu, Z. Y. *Chem. Geol.* **2009**, *268*, 74.
- (36) Paclawski, K.; Zajac, D. A.; Borowiec, M.; Kapusta, C.; Fitzner, K. *J. Phys. Chem. A* **2010**, *114*, 11943.
- (37) Gaudet, J.; Bando, K. K.; Song, Z.; Fujitani, T.; Zhang, W.; Su, D. S.; Oyama, S. T. *J. Catal.* **2011**, *280*, 40.
- (38) Ma, Q.; Divan, R.; Mancini, D. C.; Keanet, D. T. *J. Phys. Chem. A* **2008**, *112*, 4568.
- (39) Chang, S. Y.; Uehara, A.; Booth, S. G.; Ignatyev, K.; Mosselmanns, J. F. W.; Dryfe, R. A. W.; Schroeder, S. L. M. *RSC Adv.* **2015**, *5*, 6912.
- (40) Yao, T.; Sun, Z. H.; Li, Y. Y.; Pan, Z. Y.; Wei, H.; Xie, Y.; Nomura, M.; Niwa, Y.; Yan, W. S.; Wu, Z. Y.; Jiang, Y.; Liu, Q. H.; Wei, S. Q. *J. Am. Chem. Soc.* **2010**, *132*, 7696.
- (41) Ohyama, J.; Teramura, K.; Higuchi, Y.; Shishido, T.; Hitomi, Y.; Kato, K.; Tanida, H.; Uruga, T.; Tanaka, T. *Chem. Phys. Chem* **2011**, *12*, 127.
- (42) Ohyama, J.; Teramura, K.; Higuchi, Y.; Shishido, T.; Hitomi, Y.; Aoki, K.; Funabiki, T.; Kadera, M.; Kato, K.; Tanida, H.; Uruga, T.; Tanaka, T. *Phys. Chem. Chem. Phys.* **2011**, *13*, 1128.
- (43) Ma, J. Y.; Zou, Y.; Jiang, Z.; Huang, W.; Li, J.; Wu, G. Z.; Huang, Y. Y.; Xu, H. J. *Phys. Chem. Chem. Phys.* **2013**, *15*, 11904.
- (44) Usher, A.; McPhail, D. C.; Brugger, J. *Geochim. Cosmochim. Acta* **2009**, *73*, 3359.
- (45) Olaya, A. J.; Méndez, M. A.; Cortes-Salazar, F.; Girault, H. H. *J. Electroanal. Chem.* **2010**, *644*, 60.
- (46) Zhou, M.; Gan, S. Y.; Zhong, L. J.; Dong, X. D.; Ulstrup, J.; Han, D. X.; Niu, L. *Phys. Chem. Chem. Phys.* **2012**, *14*, 3659.
- (47) Kakiuchi, T. *Equilibrium electric potential between two immiscible electrolyte solutions (chap. 1)* in *Liquid-Liquid Interfaces Theory and methods*; Volkov, A.G., Deamer, D.W. Eds., CRC Press, 1996.
- (48) Duong, Q.; Tan, Y. S.; Corey, J.; Anz, S.; Sun, P. J. *Phys. Chem. C* **2015**, *119*, 10365.
- (49) Mirceski, V.; Aleksovska, A.; Pejova, B.; Ivanovski, V.; Mitrova, B.; Mitreska, N.; Gulaboski, R. *Electrochem. Commun.* **2014**, *39*, 5.
- (50) Hotta, H.; Akagi, N.; Sugihara, T.; Ichikawa, S.; Osakai, T. *Electrochem. Commun.* **2002**, *4*, 472.
- (51) E, X. T. F.; Zhang, Y.; Zou, J. J.; Zhang, X. W.; Wang, L. *Mater. Lett.* **2014**, *118*, 196.
- (52) Yoshida, Y.; Yoshida, Z.; Aoyagi, H.; Kitatsuji, Y.; Uehara, A.; Kihara, S. *Analytica. Chimica. Acta* **2002**, *452*, 149.
- (53) Taylor, G.; Girault, H. H. *J. Electroanal. Chem.* **1986**, *208*, 179.
- (54) Osborne, M. C.; Shao, Y.; Pereira, C. M.; Girault, H. H. *J. Electroanal. Chem.* **1994**, *364*, 155.
- (55) Ohde, H.; Uehara, A.; Yoshida, Y.; Maeda, K.; Kihara, S. *J. Electroanal. Chem.* **2001**, *496*, 110.
- (56) Parker, A. J. *Chemical Reviews* **1969**, *69*, 1.
- (57) Mosselmanns, J. F. W.; Quinn, P. D.; Dent, A. J.; Cavill, S. A.; Moreno, S. D.; Peach, A.; Leicester, P. J.; Keylock, S. J.; Gregory, S. R.; Atkinson, K. D.; Rosell, J. R. *J. Synchrotron Radiat.* **2009**, *16*, 818.
- (58) Dent, A. J.; Cibin, G.; Ramos, S.; Smith, A. D.; Scott, S. M.; Varandas, L.; Pearson, M. R.; Krumpa, N. A.; Jones, C. P.; Robbins, P. E. *Bi8: A core XAS spectroscopy beamline for Diamond in 14th J. Phys. Conf. Ser.* **2009**, *190*, 012039.
- (59) Ravel, B.; Newville, M. *J. Synchrotron Radiat.* **2005**, *12*, 537.
- (60) Schneider, C. A.; Rasband, W. S.; Eliceiri, K. W. *Nat. Methods* **2012**, *9*, 671.

Brust-Schiffrin synthesis

